

# Development of Background-Oriented Schlieren for NASA Langley Research Center Ground Test Facilities

Brett F. Bathel,<sup>1</sup> Stephen Borg,<sup>2</sup> Stephen Jones,<sup>3</sup> Austin Overmeyer,<sup>4</sup> Eric Walker,<sup>5</sup> and William Goad<sup>6</sup>  
*NASA Langley Research Center, Hampton, Virginia, 23681*

Michelle Clem<sup>7</sup>  
*NASA Glenn Research Center, Cleveland, Ohio, 44135*

Edward T. Schairer<sup>8</sup>  
*NASA Ames Research Center, Moffett Field, California, 94035*

*and*

Toshiharu Mizukaki<sup>9</sup>  
*Tokai University, Hiratsuka, Kanagawa, Japan, 259-1292*

**This paper provides an overview of recent wind tunnel tests performed at the NASA Langley Research Center where the Background-Oriented Schlieren (BOS) technique was used to provide information pertaining to flowfield density disturbances. The facilities in which the BOS technique was applied included the National Transonic Facility (NTF), Transonic Dynamics Tunnel (TDT), 31-Inch Mach 10 Air Tunnel, 15-Inch Mach 6 High-Temperature Air Tunnel, Rotor Test Cell at the 14×22 Subsonic Tunnel, and a 13-Inch Low-Speed Tunnel.**

## **I. Background-Oriented Schlieren Testing at NASA Langley Research Center**

Background-Oriented Schlieren is an imaging technique that is sensitive to gradients in a density field. This sensitivity comes from the dependence of the refractive index on the density field provided by the Gladstone-Dale relation.<sup>1</sup> By imaging a randomized pattern located behind the density field of interest, the path-averaged refractive index field can be ascertained by measuring the perceived displacement of the pattern (caused by changes in index of refraction) relative to a template background image, taken while wind tunnel is not running. While the operational principle of the BOS technique similar to that of a conventional schlieren imaging system, it has the capability of providing data pertaining to density fields in facilities where conventional schlieren may not be possible or practical. For instance, the BOS technique does not require a clear line-of-sight between a light source and imaging sensor (which is required for a conventional schlieren system), therefore density field information can be obtained in a ground test facility where only one point of optical access exists. The BOS technique also does not require a collimated light source, therefore imaging of the density field can be performed through windows with a lower quality (e.g. uneven surface finish, surface and internal imperfections, etc.) relative to schlieren-grade windows. Additionally, since BOS does not require a collimated light source, density field imaging can be performed over much larger fields-of-view relative to conventional schlieren imaging (where the field-of-view is limited by the size of the focusing mirrors). The

---

<sup>1</sup> Research Engineer, Advanced Measurements and Data Systems Branch, MS 493, Senior Member AIAA.

<sup>2</sup> Research Engineer, Advanced Measurements and Data Systems Branch, MS 493.

<sup>3</sup> Research Technician, Advanced Measurements and Data Systems Branch, MS 493.

<sup>4</sup> Research Engineer, US Army Aviation Development Directorate, Joint Research Project Office, MS 286.

<sup>5</sup> Research Aerospace Engineer, Configuration Aerodynamics Branch, Senior Member AIAA.

<sup>6</sup> Instrumentation Technician, Jacobs Sverdrup, MS 267.

<sup>7</sup> Research Engineer, Optics and Photonics Branch, 21000 Brookpark Rd, Member AIAA.

<sup>8</sup> Aerospace Engineer, Experimental Aero-Physics Branch, MS 260-1.

<sup>9</sup> Professor, Department of Aeronautics and Astronautics, 4-1, Kitakaname, Senior Member AIAA.

BOS technique also has the capability to provide *quantitative* density information, as the pattern displacements can be related to the strength of density gradients present in the flowfield.

This paper provides details on recent wind tunnel entries at the NASA Langley Research Center involving the application of the Background-Oriented Schlieren (BOS) technique in several of Langley’s ground test facilities. For many of the tests described in this paper, the work was performed in collaboration with participants from NASA centers other than Langley through NASA’s Aeronautical Sciences Project, Aeronautics Test Program, and Advanced Schlieren Working Group. For each of the test entries discussed in this paper, a brief description of facility operational capability is provided along with a description of the test article used to generate density disturbances imaged using the BOS technique. For some of the entries, conventional schlieren and shadowgraph imaging was also performed to provide a benchmark against which the sensitivity of the BOS technique was gauged. The purpose of this paper is to both document the primary results of these test entries as well as provide some guidance for future test entries in these, as well as other capability-related, ground test facilities where the BOS technique will be used in order to optimize the sensitivity of the technique.

### A. National Transonic Facility

The National Transonic Facility (NTF) at NASA Langley Research Center is a closed-circuit, large-scale (8.2-ft-by-8.2-ft cross section, 25-ft length test section) transonic test facility capable of providing the highest Reynolds number testing in the world.<sup>2</sup> This high Reynolds number capability is achieved in part by the introduction of evaporated cryogenic liquid nitrogen (LN2) into the test circuit to decrease flow viscosity. The introduction of evaporated LN2 allows for freestream temperatures as low as 116 K in the test section. The ability to pressurize the test section over a range of 1-atm to 9-atm at such low temperatures allows for added increase in freestream density.<sup>3</sup>

During a recent test in the NTF, retro-reflective background-oriented Schlieren (RBOS) was employed to qualitatively assess the shear layer of a capsule wake. Computational analysis showed that the wake size and shape are highly sensitive to the selection of turbulence model. The original goal of the RBOS application was to visualize the maximum width of the wake and its closure point. While the overall objectives of capturing the primary wake dimensions were not met due to technical difficulties experienced in the cryogenic environment, the images acquired in the proximity of the body clearly delineated the wake structure. This clarity of the shear layer was attributed to the density of the test medium at cryogenic temperatures.

The RBOS technique used sheets of Scotchlite 900X speckled with black latex paint. These sheets were cut into 8-inch square tiles to avoid thermal contraction and expansion issues. The tiles were then affixed to the wall, avoiding wall pressure taps and other obstacles, to create a 5-foot by 8-foot background. Figure 1 shows a region of the final latex-patterned Scotchlite 900X sidewall in the NTF (top) and the unmodified sidewall (bottom). The 900X material was selected after testing coupons of retro-reflective material in the cryogenic environment. Scotchlite 3000X was also tested, but it severely delaminated after 3 cryogenic cycles. Low static pressures generated in the test section caused the 3000X adhesive material to bubble in the proximity of fasteners and other places that air was trapped. Even after gluing the edges, the 3000X adhesive material had a difficult time remaining attached for the duration of the test. A better solution is needed for the background for future tests.

Other issues were experienced with lighting. Ring lights mounted around the camera lens were employed as the primary light source for the method. To capture the near body shear layer and extents of the wake, two cameras were used. One was zoomed in on the shoulder region of the capsule and the other was set for the larger viewing area of the wake. The zoomed in camera was electronically binned to match the pixel density of the larger camera so the same speckle size could be used for the entire background. Light return into the camera from the inner surface of the far side of the window prevented the full wake from being imaged. This camera was adjusted to eliminate the reflection issue but was unable to detect a pixel shift.

### B. Transonic Dynamics Tunnel

The Transonic Dynamics Tunnel (TDT) at NASA Langley Research Center is a transonic, closed loop, continuous flow facility with a 16×16 foot square test section capable of running



**Fig. 1:** Randomized dot pattern (top) applied to starboard wall (bottom) of National Transonic Facility for capsule wake RBOS test.

either air or the heavy gas R-134a and was specifically designed for aeroelastic testing.<sup>4</sup> The facility has an operational range extending up to nearly Mach 1.2, although this range is dependent upon the operational stagnation pressure. Details on the operational boundaries of this facility can be found in Ref. 5.

For the 1.5-day entry described in this paper, a series of initial tests were performed to determine if optical BOS measurements could be made from the control room through the multiple layers of protective glass separating the control room from the test section. Since the facility is capable of operating at stagnation pressures ranging from 0.35 psia to 15.3 psia, and because the facility is designed for aeroelastic testing that may result in collisions between a model and the tunnel sidewall, two sets of thick protective windows are installed between the test section and control room to maintain sub-atmospheric pressure and ensure the safety of the tunnel operating staff. Unfortunately, the window materials limit the optical access between the control room to the test section, making it difficult to perform optical measurements from the control room. While environmental chambers are often used to house cameras and illumination sources within the walls of the test section, these require an additional layer of complexity to implement relative to simply imaging from the control room.

For the entry described here, two specific tests were conducted to determine the feasibility of using BOS imaging from the control room. The first test used a randomized laser speckle pattern as the BOS background. The laser speckle pattern was generated inside of the control room using (in series) a single 5-mW green laser diode (Z-Laser) followed by 35-mm spherical lens and a 50-mm-diameter 10° Diffusing Angle Holographic diffuser (Edmund Optics). The pattern was aligned using a 50/50 beam splitter and passed through the control room window to illuminate a portion of the test section wall (approximately 18 feet away) covered with a 3M 8830 retroreflective material. The light was directed back towards its source from the retroreflective material and passed back through the window to the beamsplitter and into the imaging camera. In order to reduce reflections off of the control room window, the optical setup was positioned to view the back wall at an approximate 15° incidence angle. The camera, a 16-bit LaVision Imager sCMOS camera operating at 100 Hz, was fitted with a Nikon variable 35 mm – 105 mm zoom lens with the focal length setting in the first test of ~75 mm and  $F\#$  of 5.6. The camera imaged both the randomized laser speckle pattern as well as a check standard probe used to measure freestream properties along the centerline of the test section during tunnel operation. The tunnel was then run in air mode for two different stagnation pressure set points (300 lbs/ft<sup>2</sup> and 1775 lbs/ft<sup>2</sup>) and a range of Mach numbers (0 – 1.1 and 0 – 0.5, respectively). Figure 2a shows the check standard probe mounted in the TDT test section. Figure 2b shows part of the optical arrangement used for the laser speckle BOS test.

For the second test, the test section was opened and a tripod mount was placed 36 inches in front of the opposing wall of the test section. This enabled several different materials to be mounted and tested as candidate BOS backgrounds including: (1) a randomized dot pattern printed on 3M 680CR retroreflective background, (2) Krylon Glitter Blast paint, (3) crumpled aluminum foil, (4) laser speckle on 3M 7610 retroreflective background. A HomeRight® Heat Pro Deluxe II variable-temperature heat gun was then mounted on the centerline of the test section between the imaging system and background mount to generate a density disturbance. Prior to testing the candidate BOS backgrounds, shadowgraph images of the heated air flow from the heat gun were acquired while slowly increasing the heat gun's temperature setting. The BOS images were then acquired with each of the candidate backgrounds once a distinguishable shadowgraph signature on the wall of the tunnel was observed, which occurred at a heat gun setting of 340 °F. Illumination for all of the BOS and shadowgraph imaging tests (with the exception of the laser speckle test) was provided by a single CBT-120-G Light Emitting Diode, or LED, (Luminus) powered by a 40-A pulsing circuit that pulsed the LED for 80 μs at 100 Hz. A 50-mm-diameter 10° Diffusing Angle Holographic diffuser

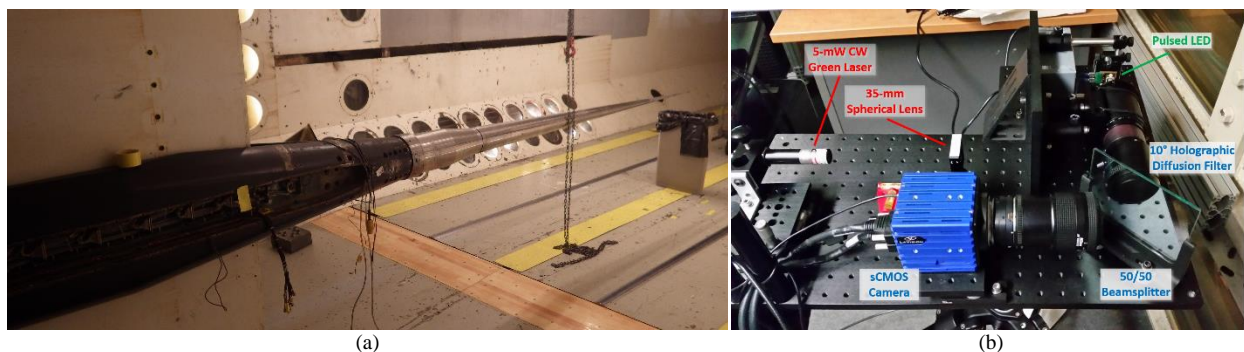


**Fig. 2:** Check standard probe mounted in test section of TDT (a) and imaging system used for both check standard test and BOS heat gun tests (b). In (b), red text denotes optics for laser speckle test, green text denotes optics for BOS and shadowgraph test, and blue text denotes optics common to both tests.

was used to disperse the light evenly across the various backgrounds. Additionally, the test section lights were on while the image data was acquired. The same 5-mW laser was used to provide speckle BOS data as was used in the first test. The camera used the same Nikon variable 35 mm – 105 mm zoom lens as in the first test, but with the focal length set to 105 mm and  $F$ -number set to 11. The camera exposure was set to 20 ms for all data shown here. Figure 2b shows part of the optical arrangement used for these heated flow BOS tests. Figure 3 shows the BOS background mount, mounted heat gun, retroreflective 3M 8830 material mounted on tunnel wall, and test section lights. As with the first test, the imaging system was mounted in the control room.

Data from the laser speckle BOS test with the check standard probe (Test 1) was processed using software developed by Edward Schairer of NASA Ames. A grid pattern of  $200 \times 400$  pixels with an interrogation window of  $16 \times 16$  pixels and 50% overlap was used to process the images. Figure 4 shows the resulting processed displacement field (with units of pixels) obtained from the Mach 1.1 condition at the 300 lbs/ft<sup>2</sup> stagnation pressure set point. The whited-out area in the imaged region represents the tip of the check standard probe. Results from single-shot images obtained during this test did not show the presence of density gradients near, or emanating from, the leading edge of the check standard probe. Similar results were obtained at a Mach 0.5 condition at a 1775 lbs/ft<sup>2</sup> stagnation pressure set point run. Based on analysis of the heated flow test (shown in Fig. 5f), it appears that the laser speckle measurement was highly susceptible to facility vibrations and time-varying laser output that altered the interference pattern imaged by the camera. When comparing Fig. 4 and Fig. 5f, the background noise levels (which appear to be on the order of 0.9 and 0.6 pixels, respectively) make it difficult to detect the presence of a weak density gradient. Note that the change in magnification between the check standard probe test and wind-off heated flow tests would result in an approximate factor of 1.7 increase in sensitivity between the former and latter. The multiple windows separating the test section from the control room, the reduced quality of those windows relative to a higher quality schlieren grade window, and oil deposits on those windows further degraded the sensitivity of the laser speckle measurement system.

Data from the heated flow tests show that when using a conventional retroreflective material with a randomized dot pattern or one of the two alternative patterns (glittered or crumpled foil), BOS measurements of a relatively weak density disturbance can be made from the TDT control room. Figures 5a and 5b show a conventional shadowgraph image obtained with the heat gun on the highest flowrate setting and a temperature setting of 340 °F both without and with a background image subtracted, respectively. Figures 5c through 5f show BOS measurements made with the patterned 3M 680CR retroreflective material, Krylon Glitter Blast, crumpled aluminum foil, and laser speckle system, respectively. Based on these single-shot images, both the conventional patterned retroreflective background and crumpled aluminum foil backgrounds appear to provide the best sensitivity. The glittered pattern also provided some sensitivity to the heated flow, however non-uniformities in the application of the glittered paint were apparent in the raw images, which contributed to reduced signal-to-noise

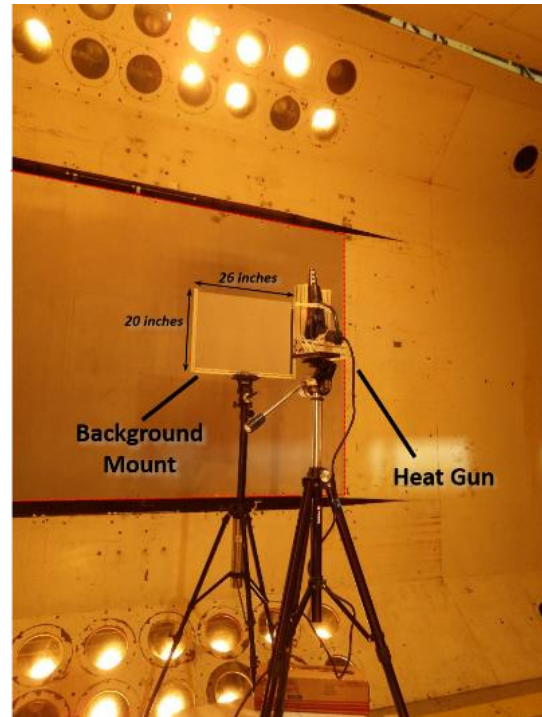


**Fig. 3:** Mount for candidate BOS backgrounds and mounted heat gun in test section of TDT. Note red dashed outline denotes location of 3M 8830 retroreflective material mounted on test section wall.

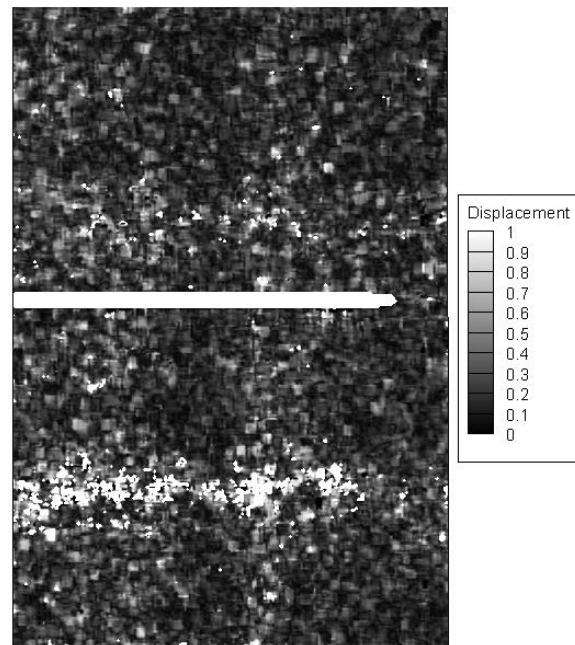


**Fig. 4:** Measured laser speckle displacement from  $M = 1.1$  check standard probe run with dynamic pressure set point of 300 lbs/ft<sup>2</sup>.

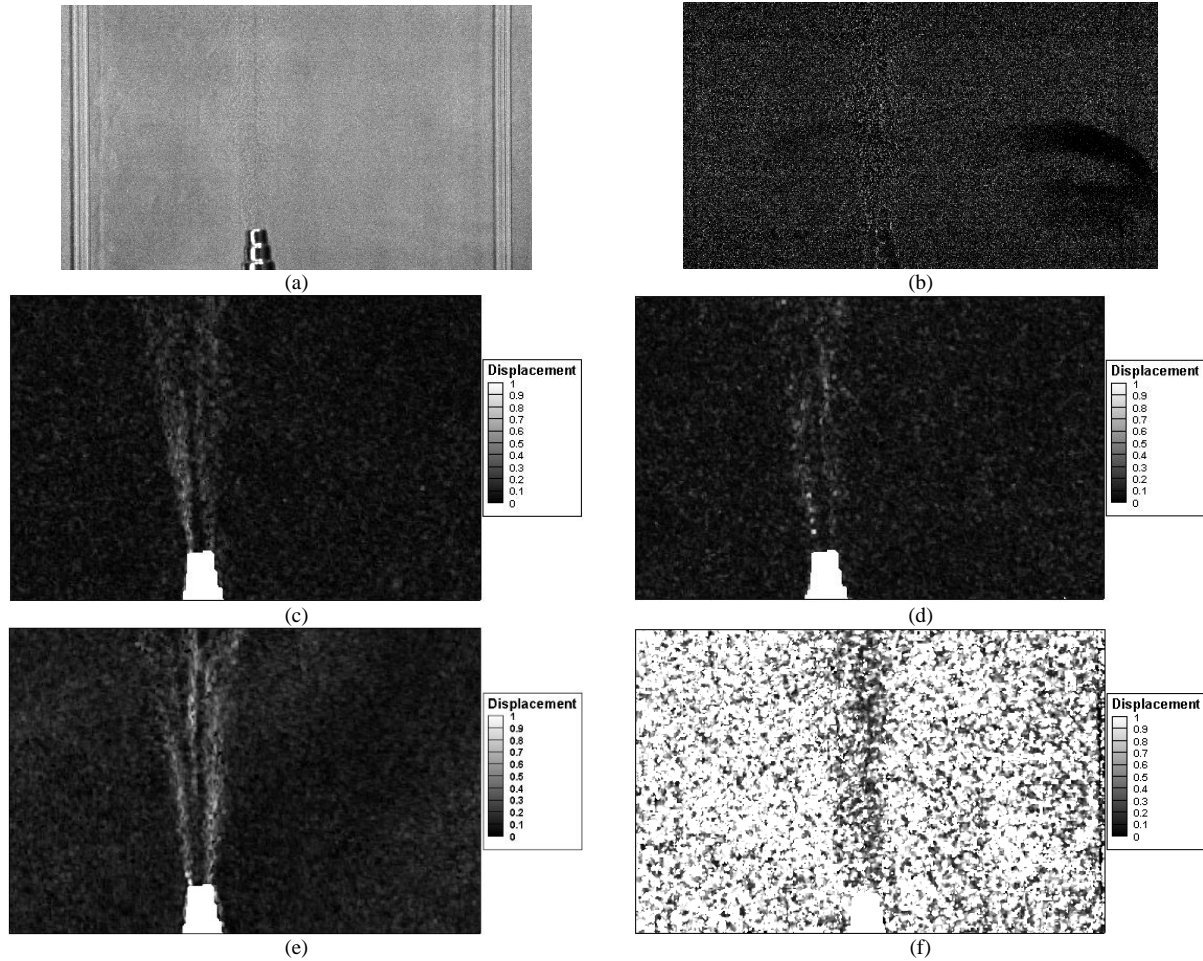


**Fig. 5:** Images of heated flow using (a) raw and (b) background-subtracted shadowgraph on TDT wall with 3M 8830, (c) BOS with random dot pattern printed on 3M 680CR, (d) BOS with Krylon Glitter Blast, (e) BOS with crumpled aluminum foil, and (f) BOS with laser speckle on 3M 7610.

levels. Further, fewer glitter elements were observed relative to measurements made in the 15-Inch Mach 6 High-Temperature Tunnel test (described in later in the paper), which reduced the spatial resolution of the measurement. This is thought to be because the incident intensity of light on the glitter pattern was much lower than that used in the 15-Inch Mach 6 High-Temperature Tunnel test. The laser speckle BOS measurement, as previously described, suffered from significant background noise that made it nearly impossible to detect the density gradient signature resulting from the heated flow.

Based on the results obtained from this entry, several improvements were identified for future BOS tests which may provide better measurement sensitivity when making measurements from the control room. The first and most obvious improvement is the use of patterned materials as backgrounds for BOS measurements in TDT as opposed to laser speckle. The complications that the facility vibrations, laser output, windows, and oil deposits on the windows present in developing a sensitive BOS measurement system can be avoided if patterned backgrounds are used. A second improvement would be to increase the magnification of the imaging system such that a smaller field-of-view is imaged by the camera. The relatively low operational pressures used during testing in TDT results in low static densities which may be hard to detect with a larger field-of-view (such as that used in this test). By increasing magnification, small density perturbations may be more easily detected.

### C. 31-Inch Mach 10 Air Tunnel

The 31-Inch Mach 10 Air Tunnel at NASA Langley Research Center was used as a preliminary demonstration of the BOS technique in a Langley hypersonic facility in September, 2012. The BOS test in 31-Inch Mach 10 Air Tunnel was performed in collaboration with researchers from NASA's Ames Research Center (Louise Walker, Edward Schairer), Glenn Research Center (Michelle Clem), as well as other participants from NASA and the DoD.

Air for the facility is supplied from a centralized bottle field to a pressurized chamber containing a 12.5 MW electrical resistance heater. The stagnation pressures inside the chamber can range from 2.41 MPa to 10.00 MPa (350 psia to 1450 psia) with a fixed stagnation temperature of 1000 K (1800 °R).<sup>6</sup> The air passes through a settling chamber and filter prior to passing through a converging-diverging contoured nozzle with a 2.72 cm (1.07 inch) square throat. The flow is accelerated to a nominal Mach number of 10 as it expands through the nozzle into a 31-inch square test section. The stated pressure fluctuations within the inviscid core flow are  $\pm 1.0\%$ .<sup>6</sup> Three large UV-transmitting windows are mounted flush to the top, side, and bottom interior walls of the test section. These windows are capable of transmitting light down to a wavelength of 190 nm. The fourth sidewall contains a sliding door that separates the wind tunnel test section from the housing for the model injection system (called the *model housing box*). Once the Mach 10 flow is established within the test section, this door is opened, and the wind tunnel model is injected into the flow via a hydraulic injection system. The sting used to support the wind tunnel model is mounted to an aerodynamic strut. This aerodynamic strut can be positioned over a wide range of pitch and yaw angles with control provided by a remote model control system.



**Fig. 6:** A CEV blunt body model used for BOS testing in the 31-Inch Mach 10 Air Tunnel in September, 2012.

A scaled Crew Exploration Vehicle (CEV) blunt body was used in the experiment and is shown in Fig. 6. In this facility, the optical access to the test articles is very good and the model can be viewed simultaneously in either the vertical or horizontal plane. For this experiment BOS was used along the horizontal orientation. The camera system and light sources were set up outside the tunnel and viewed the model along the axis of the model injection plate. A randomized dot pattern consisting of black dots over a retroreflective base layer was painted on the model injection plate. A 12.3 MegaPixel (MP) Nikon D300S camera with a pixel array measuring 4288×2848 pixels using a DX formatted Complimentary Metal-Oxide Semiconductor (CMOS) sensor (23.6-mm by 15.8-mm) and a Nikkor 35 mm lens was used to image the model. In this configuration, with a camera-injection plate distance of approximately 38 inches, a background pattern of approximately 0.5 mm (0.02 inch) diameter targets was required. The retro-reflective base layer was made up of six coats of Axon Hentzen silver white Alert - #1440 paint, and applied directly to the model injection plate. The dots were then sprayed over the base layer using a 10% diluted solution of water-based latex paint (Valspar Ultra interior flat black #007.0391621) and a calibrated paint sprayer. A uniform field of 0.5 mm (0.02 inches) diameter dots was produced using a liquid pressure of 25 psig and an air pressure of 10 psig.

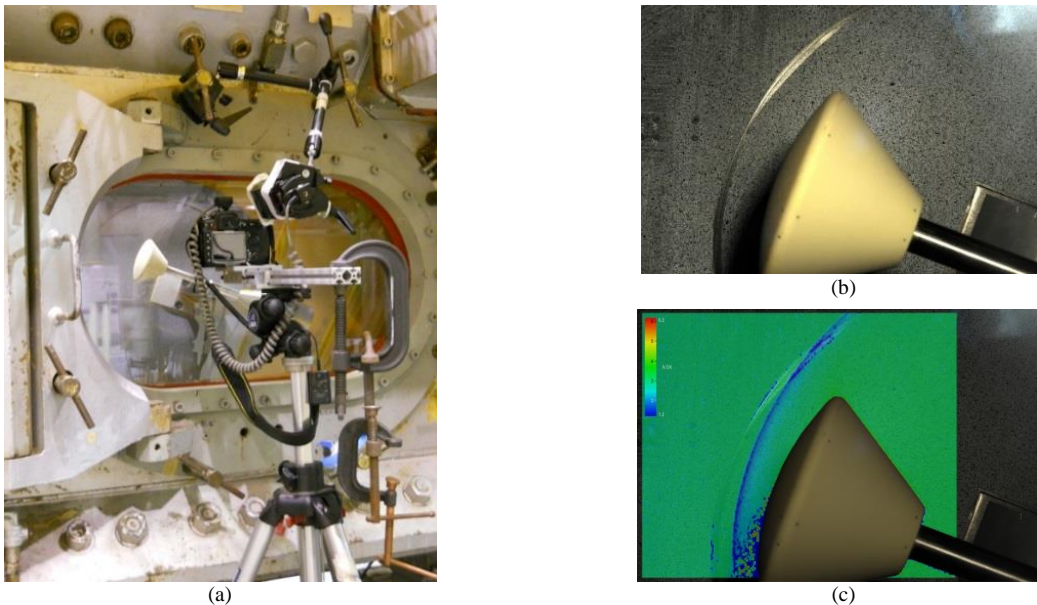


**Fig. 7:** View of the injected model, camera and lighting as configured in the 31-Inch Mach 10 Air Tunnel (a), unprocessed image data of the CEV-type blunt body (b), processed BOS data showing DX pixel displacements superimposed onto the original image (c).

Figure 7 shows (a) the experimental setup, (b) the unprocessed CEV image, and (c) the processed data overlaid onto the original image. For these data, a single wind-on/wind-off image pair was used in the calculation of the BOS pixel shifts. The raw image files were formatted as 8-bit grey-scale images and then processed using software developed by Edward Schairer (Ames Research Center). The pixel shift data was generated using an interrogation window size of  $32 \times 32$  pixels and 50% window-window overlap, then overlaid back onto the original wind-on image for clarity. The bow shock shown on the CEV blunt body in Figure 7c loses a portion of its well-defined edge due to uneven lighting conditions in the test section. A shadow of the model was projected onto the injection plate as shown in Figure 7b, preventing the pixel shift data from being detected during post-processing.

While the bow shock was clearly imaged in Fig. 7c, several flow features typically present in such hypersonic flowfields were not imaged, such as shear layers and expansion fans. The inability to image such flow features can probably be partially attributed to the relatively low densities characteristic of this hypersonic flowfield. However, limitations of the imaging system used in this experiment most likely contributed to a lack of sensitivity to these flow features. The first limitation of the imaging system was the use of 8-bit images that affect the ability of the cross-correlation software to measure sub-pixel displacements. Second, the use of a relatively short focal length lens to image the flowfield limited the sensitivity of the imaging system. Had a higher focal length lens been used, flow features such as the shear layers and expansion fans would have been more highly magnified, resulting in better BOS imaging sensitivity to those features.

#### D. 15-Inch Mach 6 High-Temperature Air Tunnel

The 15-Inch Mach 6 High-Temperature Air Tunnel at NASA Langley Research Center was used in October 2014 to again demonstrate the feasibility of the BOS technique when applied to a hypersonic flowfield measurement. During this entry, unconventional background patterns were tested to assess their performance relative to a conventional background (consisting of retroreflective material with a randomized printed dot pattern). Both conventional shadowgraph and high-speed schlieren measurements were also performed to gauge the effectiveness of the BOS technique in identifying density gradients present within the hypersonic flowfield. This test was performed in collaboration with NASA Glenn Research Center (Michelle Clem).

Similar to the 31-Inch Mach 10 Air Tunnel, air for the 15-Inch Mach 6 facility is supplied from a centralized bottle field to a pressurized chamber containing a 5 MW electrical resistance heater. The stagnation pressures inside the chamber can range from 0.35 MPa to 3.10 MPa (50 psia to 450 psia) with a variable stagnation temperature of 522 K – 700 K (940 °R – 1260 °R).<sup>7</sup> The air passes through a settling chamber and filter prior to passing through a converging-diverging contoured axi-symmetric nozzle with a 4.60 cm (1.81 inch) throat<sup>6</sup> and 37.01 cm (14.57 inch) exit diameter. The flow is accelerated to a nominal Mach number of 6 at the nozzle exit where it passes through the vacuum chamber, passing over the model (if present), and is finally collected 18 inches downstream by a diffuser with a 64.8 cm (25.5 inch) entrance diameter. The vacuum chamber itself is approximately 83-inches-wide by 96-inches-tall. A large 48-inch-wide by 67- $\frac{1}{4}$ -inch-tall stainless steel door on the port-side of the chamber is used to mount a 30-inch-wide by 24-inch-tall schlieren-quality window. An identical window is mounted to a sliding door on the opposite side of the tunnel. Additional optical access is available through a similar window on the top of the tunnel and through two sets of round windows mounted diagonally near the top of the chamber. The floor of the vacuum chamber serves as the support for the model injection system. Once the Mach 6 flow is established within the test section, hydraulic actuators insert the sting-mounted model into the core flow. Figure 8 shows a picture of the 15-Inch Mach 6 facility with the portside door open (a) and a view of the model from the starboard side of the tunnel (b).

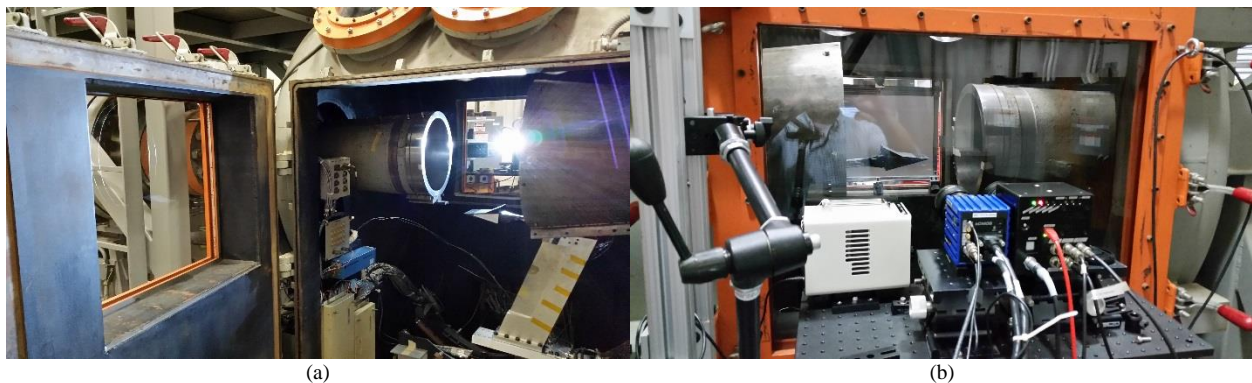


**Fig. 8:** View of retracted model from port-side of vacuum chamber (a) and view from opposing side of chamber showing injected model with imaging cameras in the foreground and retro-reflective panel mounted inside the chamber in the background (b).

For the 15-Inch Mach 6 High-Temperature Air Tunnel BOS experiment, a single 20° wedge model with a sharp leading edge was used to generate a series of shock and expansion waves. The upper surface of the wedge model, over which the BOS measurements, schlieren, and shadowgraph visualizations were made, consisted of two surfaces. The first surface was a nearly solid piece of stainless steel with a 20° wedge and a sharp leading edge. This wedge had a plenum machined into the upper surface that was covered by a flat stainless steel insert with an 11-mm-long by 0.81-mm-wide slot used for seeding air

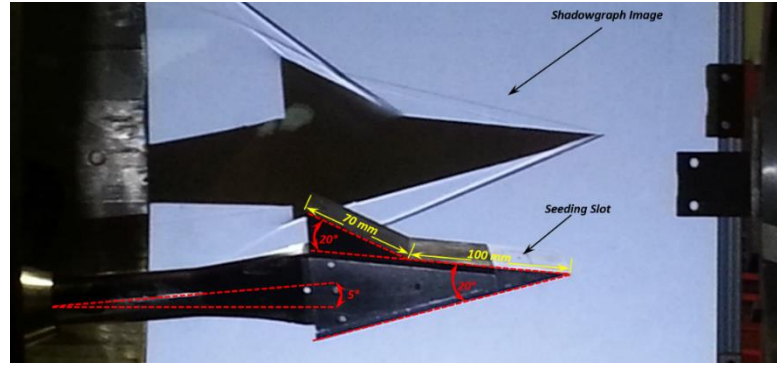


**Fig. 9:** Wedge model (foreground) with dimensions as viewed from the starboard side of the 15-Inch Mach 6 High-Temperature Air Tunnel. Shadowgraph image is observed on the background retroreflective panel. Flow is from right to left.

into the boundary layer. This slot was centered on the model's spanwise line of symmetry 29.4 mm downstream of the leading edge. A 0.76-mm-diameter pressure port was also machined into the top surface of the wedge. This port was 33.3 mm downstream of the leading edge and 23.1 mm from the model's port-side edge. The second surface was a stainless steel 20° compression corner insert that mounted to the top of the wedge model. This insert was butted up against the aft end of the leading 20° wedge. The first 52 mm of this insert was flat and nearly flush with the leading wedge's surface, although a slight forward step, ranging between 0.014-inches to 0.024-inches, existed at this junction. At 52 mm (100 mm downstream of the leading edge), an abrupt 20° incline extended an additional 70 mm. The spanwise width of the model, including both of these surfaces, was a constant 127.0 mm. Each of the surfaces was painted with a flat black high temperature paint to minimize light scatter. Figure 9 shows a side view (starboard) of the model during a shadowgraph wind tunnel run with relative dimensions shown. For each run described in this paper, the sting of the model was pitched 5°, resulting in an initial *plate angle* of 5°.

Figure 10 shows time-averaged results obtained using (a) conventional schlieren, (b) conventional shadowgraph on a 3M 7610 retroreflective background, (c) BOS with a randomized dot pattern printed onto a 3M 680CR retroreflective background, (d) BOS with a random glitter pattern, (e) BOS with a crumpled aluminum foil background, and (f) BOS with a laser speckle pattern projected onto a 3M 7610 retroreflective background. Table 1 provides tunnel operation details for each run. Table 2 provides details on instrumentation for those runs. For the conventional, glittered, and foil background BOS runs, listed in Table 2, dual gooseneck fiber optic attachments (AmScope) were used to better illuminate the backgrounds.

All images shown in Fig. 10 were obtained with a 16-bit LaVision Imager sCMOS camera operating at 100 Hz. A Photron FASTCAM Mini UX100 camera was also used in the BOS and shadowgraph runs of this test and a Phantom v12 CMOS camera used for the schlieren runs, however only images from the LaVision camera are presented in this paper. Initial post-processing of images shown here was performed using ImageJ, a freeware image-processing program available from the National Institutes of Health.<sup>8</sup> For the schlieren image shown in Fig. 10a, the first 45 images obtained during the run were averaged and a time-averaged background image (obtained while the tunnel was not running) was subtracted to produce the final image. The shadowgraph image in Fig. 10b was obtained in a similar manner, however the first 100 images obtained during the run were time-averaged, a time-averaged background was subtracted, and the intensity distribution inverted to produce the final image. The time-averaged schlieren and shadowgraph images were meant to serve as benchmarks against which the quality of the BOS measurements could be gauged. For the BOS and shadowgraph runs, the camera was mounted just outside the window on the starboard side of the tunnel and the background was mounted just inside the window on the port side of the tunnel, with an approximate distance of 83 inches between the two. The model was located approximately halfway between the camera and background (see Fig. 8b).

**Table 1:** Approximate tunnel conditions for 15-Inch Mach 6 High-Temperature Air Tunnel BOS entry.

Technique	Figure	P <sub>0</sub> (MPa)	T <sub>0</sub> (K)	P <sub>2</sub> (kPa)	T <sub>2</sub> (K)
Schlieren	10a	2.59	482.1	3.04	314.4
Shadowgraph	10b	2.70	461.6	3.28	326.8
Conventional BOS	10c	2.50	501.9	3.04	322.0
Glitter BOS	10d	2.54	507.8	3.11	332.6
Foil BOS	10e	2.59*	505.4*	-	-
Laser Speckle BOS	10f	2.58	490.3	3.18	314.3

\* Data acquisition system did not trigger for this run, therefore nominal value is reported.

**Table 2:** Run details for 15-Inch Mach 6 High-Temperature Air Tunnel BOS entry.

Technique (Figure)	Light Source (Manufacturer)	Source Type	Camera Exposure (ms)	Lens Parameters	Background	Pattern
Schlieren (10a)	1 CBT-120-G LED (Luminus)	Pulsed ( $\tau_{pulse} = 2\mu s$ )	0.05	$f = 105$ mm $F\# = 2$	N.A.	N.A.
Shadowgraph (10b)	1 30-W LED (AmScope)	Continuous	1.00	$f \approx 55$ mm $F\# = 3.5$	3M 7610	N.A.
Conventional BOS (10c)	3 50-W LEDs (AmScope)	Continuous	0.10	$f \approx 55$ mm $F\# = 16$	3M 680CR	Printed dots
Glitter BOS (10d)	3 50-W LEDs (AmScope)	Continuous	2.00	$f \approx 55$ mm $F\# = 16$	High Heat Black (Rustoleum)	Glitter Blast (Krylon)
Foil BOS (10e)	3 50-W LEDs (AmScope)	Continuous	0.49	$f \approx 55$ mm $F\# = 16$	Aluminum Foil	Crumples
Laser Speckle BOS (10f)	1 5-mW Green Laser (Z-Laser)	Continuous	19.50	$f \approx 55$ mm $F\# = 16$	3M 7610	Laser Speckle
	1 1.5-mW Green Laser (Melles-Griot)					

For BOS Figs. 10c through 10e, the first 100 images acquired during a run were averaged and then processed to obtain the magnitude of pixel displacement relative to a background image. For the laser speckle BOS measurement shown in Fig. 10f, two sequential frames near the end of the run were averaged and processed relative to a background image consisting of an average of two sequential images acquired soon after the model was retracted from the core flow. This alternative processing method for the laser speckle BOS run was necessary because the speckle pattern changed significantly during the course of the run, preventing the use of a background obtained before or after the run. This time-varying speckle pattern is thought to be a consequence of facility vibration and the varying output of the laser source. Unfortunately, the selected laser speckle BOS images are from a period in the run during which pressurized air ( $\sim 125$  psi) was supplied to the seeding slot. However, the primary features of that flowfield are similar to those when the air was off.

In Figs. 10c through 10e, the results obtained using the conventional pattern, glitter pattern, and crumpled foil pattern appear qualitatively similar. For all BOS runs, a grid pattern of  $1200 \times 600$  pixels with an interrogation window of  $16 \times 16$  pixels with 50% overlap was used to process the images using software developed by Edward Schairer of NASA Ames. A noticeable, but relatively small difference between the conventional and unconventional (glitter and foil) backgrounds was the baseline noise level, which was slightly higher for the unconventional backgrounds. This is

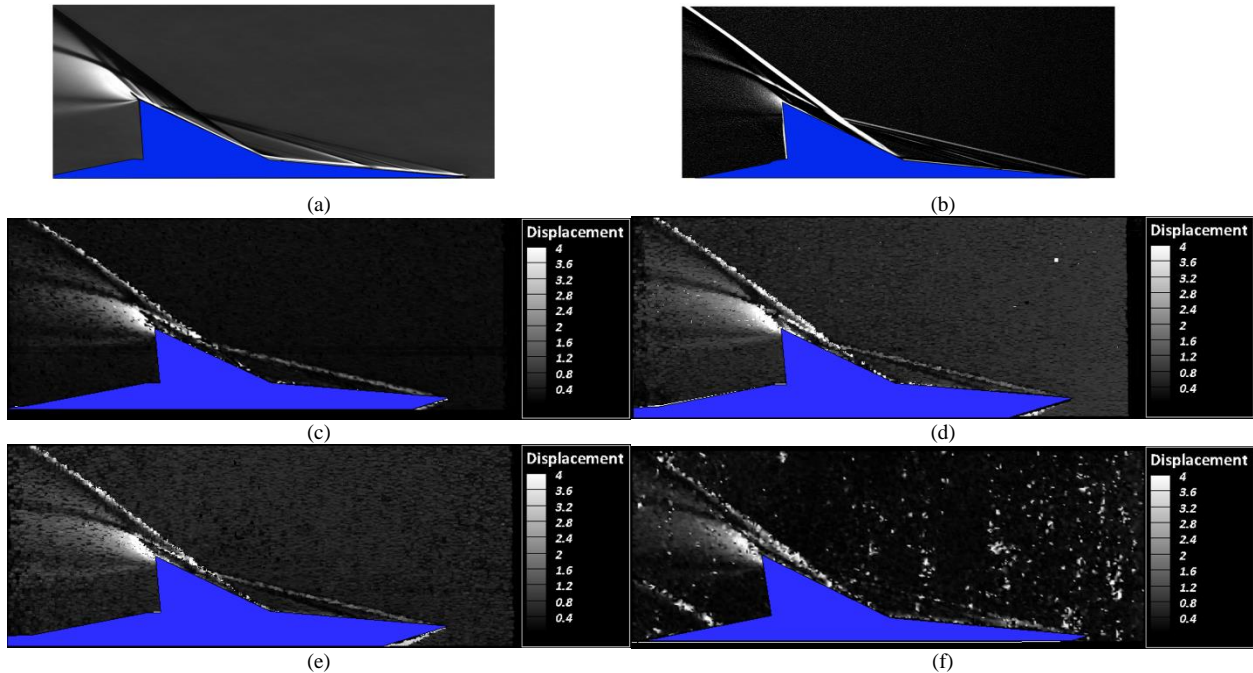


**Fig. 10:** Times-averaged digital images obtained from 15-Inch Mach 6 High-Temperature Air Tunnel using (a) conventional Schlieren, (b) conventional shadowgraph, (c) BOS with conventional background, (d) BOS using painted glitter background, (e) BOS using crumpled foil background, and (f) BOS using low-power CW lasers to produce speckle pattern.

thought to be due to small variations in the reflected light pattern from the unconventional backgrounds induced by either facility vibrations, a result of the processing algorithm, or a combination of the two. Unlike the conventional background, where facility vibrations result in a uniform translation of the background that can be accounted for in post-processing, facility vibrations may result in significant changes in the reflected light pattern from the unconventional backgrounds (similar to an illuminated rotating disco ball). A benefit of using either the glitter or crumpled foil pattern when compared to the conventional retroreflective background with a randomized dot pattern is the lower relative cost and simplicity of application. The results obtained using the laser speckle pattern in Fig. 10f were of significantly lower quality than the results obtained with the other BOS backgrounds. This was thought to be the result of multiple factors, most notably being facility vibrations influencing the speckle pattern during both the run and when the facility was not running.

While the BOS results obtained using the various background patterns did not match the spatial resolution and detail of the benchmark schlieren and shadowgraph images, many of the complex features of the flowfield were captured with the BOS methods. In future experiments, if both higher spatial frequency background patterns and higher imaging magnifications are used, better spatial resolutions can be achieved and more complex flow patterns imaged. Additionally, by adequately isolating the camera, illumination source, and background from facility vibrations, improvements in signal-to-noise ratio may be realized. The use of higher intensity pulsed lighting may also increase the fidelity of the BOS measurements relative to the benchmark schlieren and shadowgraph results by reducing the effective exposure of the camera and limiting the amount of image blur. One noted benefit of using the glitter and crumpled foil backgrounds in this experiment was that both patterns were unaffected by the near-vacuum pressures in the test section. When testing with the 3M 680CR background, some areas of the material bubbled up when subjected to the near-vacuum environment.

#### **E. Rotor Test Cell at the 14×22 Subsonic Tunnel**

The Rotor Test Cell (RTC) within the 14×22 Subsonic Wind Tunnel at NASA Langley Research Center was used to demonstrate the usefulness of the BOS technique in detecting vortices shed by rotor blades when the rotorcraft vehicle was in ground effect. Conventional shadowgraph was also used to track the vortices and provide a comparative measurement. This test was performed in collaboration with NASA Ames Research Center (Edward Schairer) and the U.S. Army Aviation Development Directorate (Austin Overmeyer).

The RTC is a chamber measuring 40-feet by 68-feet and 43-feet tall. The ground plane was formed by a spare model cart that measured approximately 21-feet by 20-feet and 10-feet high. The test used the Army's General Rotor Model System (GRMS), which is a rotor drive system that is able to be fully contained within a fuselage. As described by Murrill,<sup>9</sup> the system uses two 75 hp (55.9 kW) water-cooled electric motors capable of driving a rotor with a diameter up to 13.1-feet. Two internal six-component strain gauge force and moment balances are used for obtaining the independent fuselage and rotor aerodynamic loads. The GRMS was mounted on a sting attached to a large model cart placing the center of the rotor over the ground plane. A four-bladed fully articulated hub with an 11.1-foot rotor diameter was used for this test. The blades were a pre-existing set of rotor blades in the Army's inventory used to represent an advanced, modern rotor with RC-series airfoils. The fuselage was the NASA ROBIN-Mod7 analytically-defined helicopter fuselage model that has been used in numerous tests prior to this entry.

For the BOS measurements, a 12-bit PCO DiMAX HD CMOS camera was mounted behind the rotorcraft vehicle on its port side with a zoom lens having an approximate focal length of 75 mm and  $F$ -number setting of 5.6. This camera was operated at 400 Hz with a 100  $\mu$ s exposure. Two Luminus CBT-120-G LEDs mounted horizontally on either side of the camera lens and pulsed by two Luminus DK-114N-1 circuits were used to illuminate the 4-foot-wide by 8-foot-tall 3M 3000X panel on the opposing side of the test cart, as shown in Fig. 11a. Two 50-mm-diameter 10° Diffusing Angle Holographic diffusers (Edmund Optics) were used to disperse the light emitted by the LEDs. Three additional Teledyne DALSA Falcon2 cameras operated at 25 Hz, each with a 100 mm focal length lens, were also used to visualize the flowfield. However, only results from the PCO DiMAX HD camera will be presented here. A close-up view of the PCO DiMAX HD camera mounted with the two pulsed LEDs and diffusion filters, along with the Falcon2 cameras mounted with their respective pulsed LED units, are shown in Fig. 11b with dimensions relative to the corner of the test stand. Shadowgraph measurements were performed to serve as a benchmark against which the BOS results could be compared. For the shadowgraph measurements, only one of the pulsed CBT-120-G LEDs was operated with the diffusion filter removed. A 48-inch-wide by 49-inch-tall panel layered with 3M Engineer Grade Prismatic Reflective 3430 white retroreflective material was mounted just in front of the BOS pattern and served as the background for the shadowgraph measurements. Figure 11c shows the dimensions of the test stand and background pattern during a test.

For both the BOS and shadowgraph runs, an image stabilization routine<sup>10</sup> in ImageJ<sup>8</sup> was applied to each run image to minimize effects of camera motion induced by the strong outwash of the test vehicle. For all BOS runs, a grid pattern

of  $126 \times 122$  pixels with an interrogation window of  $32 \times 32$  pixels and 50% overlap was used to process the images using software developed by Edward Schairer of NASA Ames. For the shadowgraph images, a background image was subtracted from the run images to minimize artifacts from the retroreflective sheeting.

Figures 12a, 12b, 12c, and 12d show BOS results obtained for thrust coefficients of  $C_T = 0.004, 0.006, 0.008,$  and  $0.009,$  respectively. In each of the images the rotor blade, traveling in the counter-clockwise direction when viewed from above the vehicle, has just passed out of the field of view in the top right-hand corner. As  $C_T$  was increased, the refractive signature of the vortices increased markedly. In Figs. 12c and 12d, vortices entrained in the downwash originating from passage of the rotor blades near the front (aligned diagonally from top-left to bottom-right) and aft

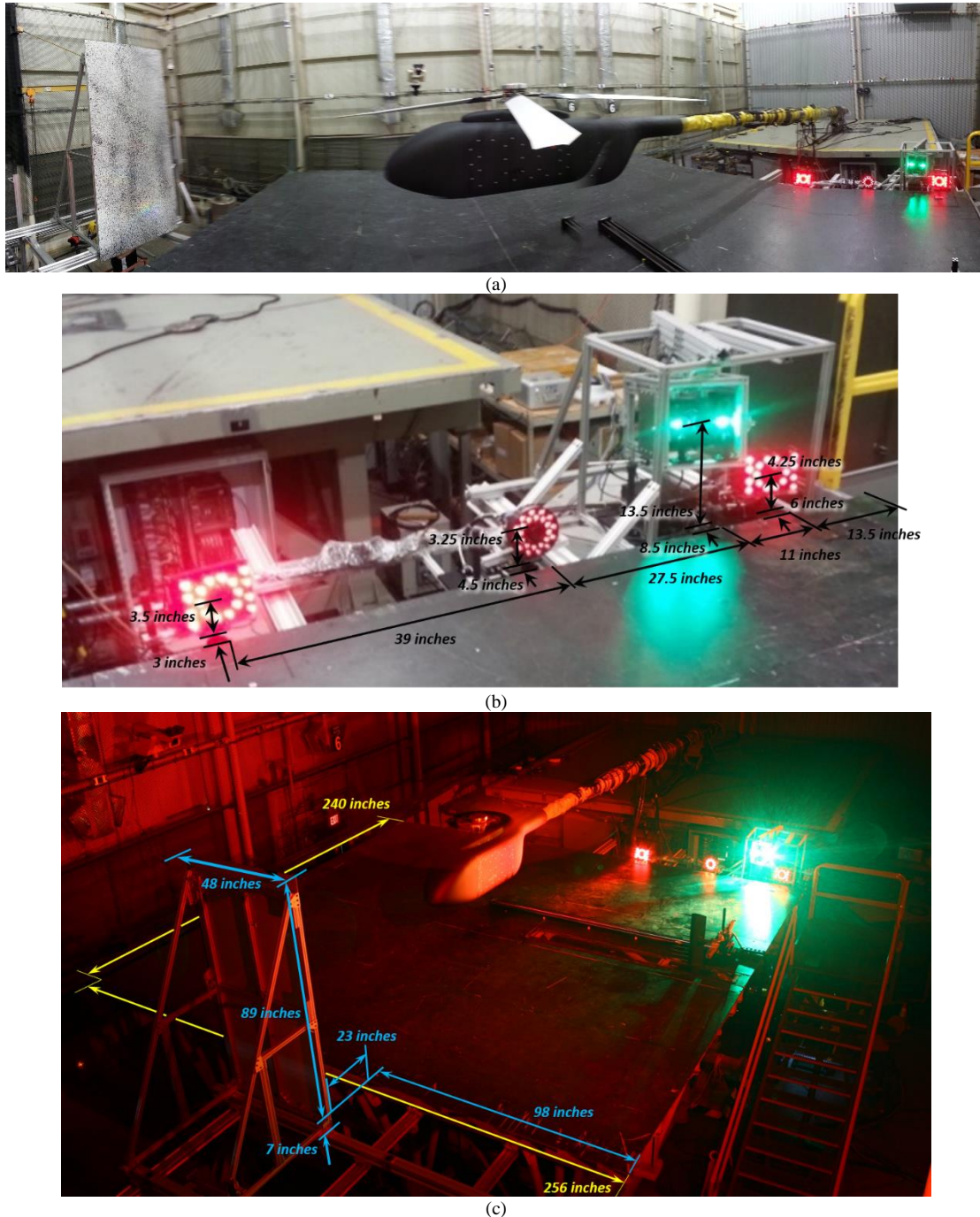


**Fig. 11:** (a) Panoramic view of rotorcraft model in Rotor Test Cell with background pattern shown to the left and camera/lighting system shown to the right. (b) View of camera and pulsed LED lighting system with dimensions. (c) View of rotorcraft model and rectangular test cart in Rotor Test Cell during a test with dimensions shown.

(aligned diagonally from bottom-left to top-right) are clearly seen. Although not apparent in the single images presented in Figs. 12a through 12d, image sequences from each run appear to show turbulence entrained in the downwash. Near the bottom 1/3 of the field of view, the apparent turbulence (and vortices at the higher  $C_T$  conditions) in downwash begin to move outward, marking the beginning outwash region of the flowfield.

Figures 12e, 12f, 12g, and 12h show shadowgraph results obtained at the same respective thrust coefficient conditions. Similar to the BOS images, the refractive signature of the vortices increased with increased  $C_T$ . In each of the images the rotor blade, again traveling in the counter-clockwise direction when viewed from above the vehicle, is shown just before it passed out of the field of view in the top right-hand corner. Unlike the BOS images, the turbulence entrained in the downwash was not observed at any of the  $C_T$  conditions. Unfortunately, the hexagonal pattern artifacts present in the retroreflective materials limited the effectiveness of the shadowgraph imaging and most likely prevented observation of the turbulence in the downwash. In future tests, a more uniform retroreflective material, such as 3M 7610, will be used to eliminate such artifacts.

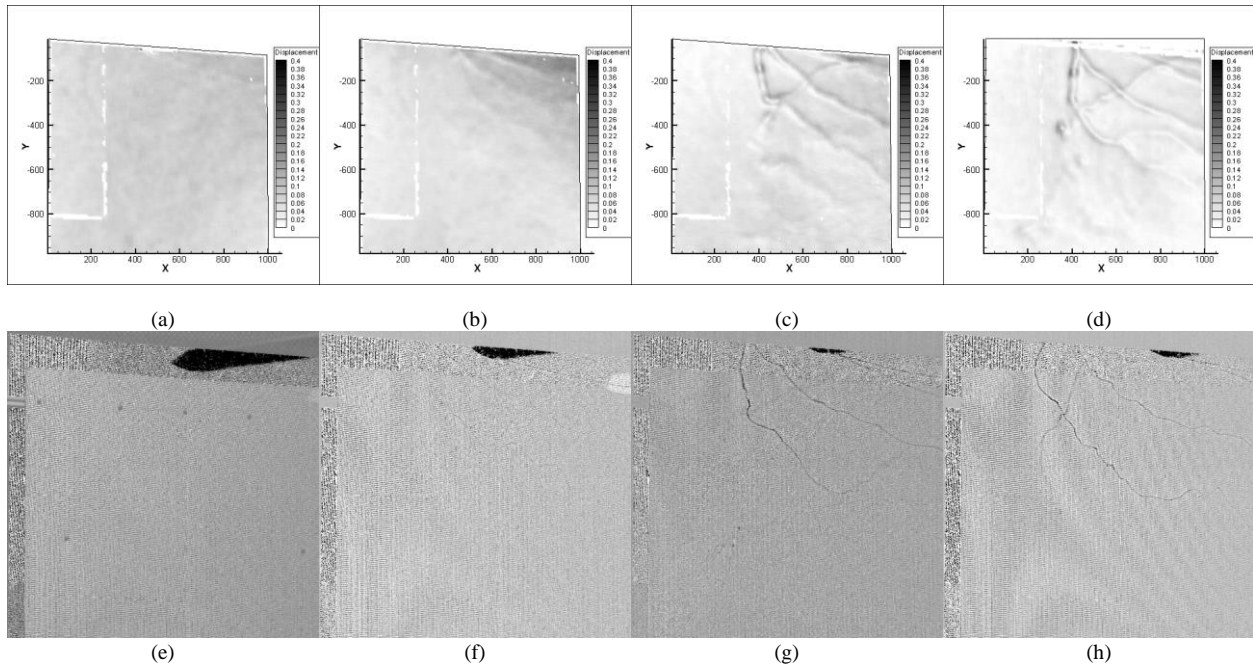


**Fig. 12:** Single Background-Oriented Schlieren (top) and shadowgraph images (bottom) for thrust coefficient values ( $C_T$ ) from left-to-right of 0.004, 0.006, 0.008, and 0.009, respectively.

While the entry at the Rotor Test Cell was successful in that vortices were observed in the downwash and outwash in both the BOS and shadowgraph imaging runs, several improvements for future imaging systems were identified that mostly likely would enhance data collection. First, the use of retroreflective materials with hexagonal or other built in patterns that do not return light from an illumination source create unwanted artifacts in the images. The use of a uniformly coated retroreflective material, such as 3M 7610, would minimize the presence of these image artifacts. Second, care must be taken during application of retroreflective materials with intensity return dependencies on orientation. In Figs. 12a through 12d, a rectangular outline on the left-hand side of the field-of-view can be seen. This outline was a consequence of a significant intensity gradient resulting from the application of that 3M 3000X sheet in an orientation where the light-reflecting elements in that material were aligned at  $90^\circ$  relative to the remaining sheets in the rest of the field-of-view. Finally, when applying a randomized pattern to the retroreflective material, great care must be taken to ensure proper sizing of the pattern (both in terms of size and spacing). Unfortunately in this test, large variations in pattern size and spacing occurred, which limited the resolution with which the vortices and entrained turbulence were visualized.

### F. 13-Inch Low Speed Tunnel

The 13-Inch Low Speed Tunnel housed within the Advanced Measurements and Data Systems Branch at NASA Langley Research Center was used demonstrate the BOS technique at low, subsonic Mach numbers and is described in detail in Ref. 11. A brief description of this test is provided below. This test was performed in collaboration with Tokai University (Toshiharu Mizukaki).

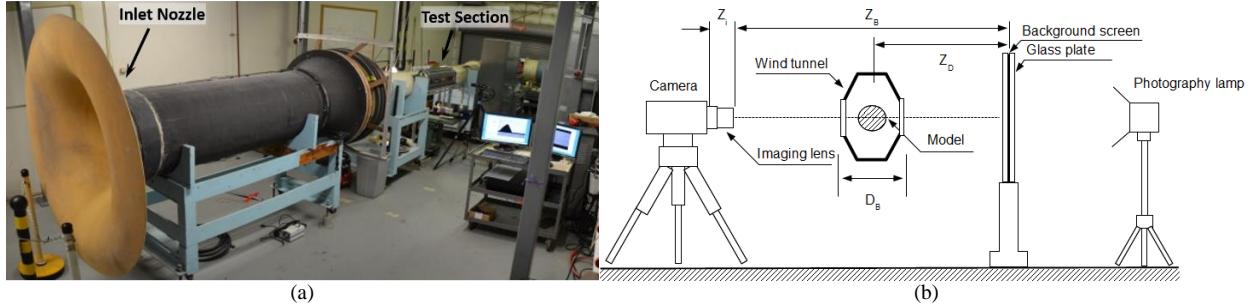


**Fig. 13:** View of (a) 13-Inch Low-Speed Tunnel showing inlet nozzle on the left and test section on the right and (b) cross-section view of test section in 13-Inch Low-Speed Tunnel showing BOS setup used for test.

The 13-inch Low Speed Tunnel is an open loop, continuous run facility which is powered by a 2 kW turbofan motor located downstream from the test section. This low-speed facility features a tapered inlet with flow conditioners upstream of the test section and can generate free-stream Mach numbers up to 0.4 and Reynolds numbers of up to ~28,000. The test section has a 13-inch diameter, octagonal cross-section with symmetric but unequal sides. The test section horizontal and 45° windows have dimensions of 1.125-inches by 36.5-inches (28.575 mm by 927.1 mm) and the vertical windows measure 3.5-inches by 36.5-inches (88.9 mm by 927.1 mm). The windows are made from a low iron content, soda-lime float glass (Starphire®) with enhanced transmissivity in the 330nm through 550nm range.

The model used in this demonstration was a cone-shaped blunt-body, visually similar but not identical to the designs used in the Apollo command module as well as NASA’s current CEV. Dimensionally this 4-inch (101.6 mm) diameter model has a heat shield radius of 1.2 times the diameter, a corner radius 0.05 times the diameter, and a 33° back-shell angle. The symmetric axis of the model is offset from the sting axis by 28° to simulate the angle of attack used during atmospheric re-entry<sup>12</sup> (Fig. 14a).

The imaging of flow phenomena in the vicinity of the heat shield corners was of primary significance, but due to the capsule’s large diameter in comparison to the test section vertical window height, only half of the model could be clearly imaged at one time. Re-orienting the model on the sting in a “cone up” and “cone down” configuration allowed us to fully map the stagnation points, corner flowfields and wake over the tested Mach number range.

BOS image data was acquired using a Teledyne Dalsa Falcon2 camera connected to a Dalsa Xcelera-CL +PX8 framegrabber. This is a 12 MP (4095×3072) CMOS sensor-based camera with an 8-bit or 10-bit pixel depth and 58 Hz or 45 Hz maximum framerate (at full field), respectively. For this experiment, image data was taken for each model orientation at Mach numbers of 0.10, 0.20, 0.30, 0.35 and 0.40. A 100 mm focal length lens at an  $F$ -number setting of 22 was used to image the flowfield. The distance between the camera and background was 32.9 inches (835 mm) and the distance between the model and background was 5.9 inches (150 mm). This spacing required the use of a 0.20 mm dot pattern as the background.

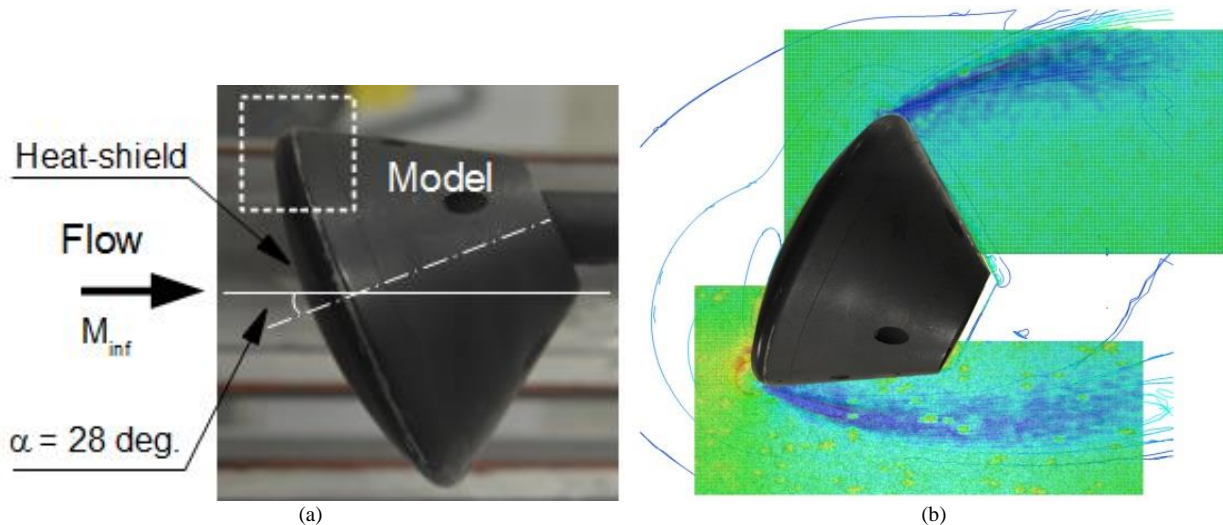


**Fig. 14:** Image (a) of CEV-type capsule used during 13-Inch Low-Speed tunnel entry and (b) BOS generated density fields around the capsule and superimposed over a CFD simulation at Mach 0.40.

BOS pixel shifts were generated from a single wind-on/wind-off image pair and processed using software developed by Edward Schairer (Ames Research Center). The pixel shift data was generated using an interrogation window size of  $16 \times 16$  pixels and 50% window-window overlap. For comparison, a separate computational fluid dynamic (CFD) simulation was run for the Mach 0.40 case and the BOS experimental data was superimposed over it (Fig. 14b). The BOS results were in good agreement with the numerical solution and able to detect the general shape of the wake density field on the top and bottom of the vehicle as well as the location of the stagnation point on the cusp of the lower shoulder. The BOS-derived flowfields around the capsule, from Mach 0.10 through Mach 0.40, are shown in Fig. 15 and the density signatures are seen to become more pronounced as the density gradient increases with Mach number.

It was noted during testing that improvements needed to be made to the light sources and their effect on the background support. During the test the image depth-of-field was maximized by increasing the  $F$ -number setting of the lens in order to improve measurement sensitivity, which consequently reduces the amount of light incident on the image sensor. Further, short camera integration times were also necessary to minimize the effects of time-averaging of high-frequency flow dynamics. The high  $F$ -number and short exposure necessitated the use high intensity lighting in order to get enough contrast in the BOS images. During this entry however, radiative heating from the high intensity lights induced warping in the back-lit randomized dot pattern, which was originally perceived as density-related shifts in the background pattern. Future tests in this facility will use high-intensity, short-pulse LEDs with much lower heat output to reduce warping in patterned backgrounds.

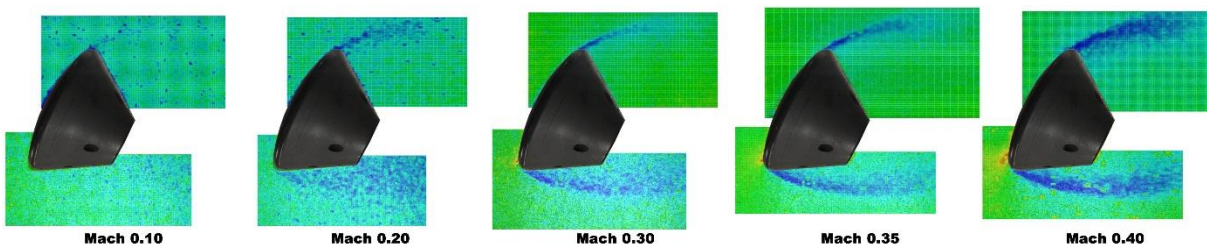


Fig. 15: BOS density-field around a CEV-type blunt body from Mach 0.10 – 0.40.

## II. Conclusions

This paper provides a summary of recent Background-Oriented Schlieren (BOS) entries in ground test facilities at the NASA Langley Research Center. For all of the entries, a description of the experimental setup, including the imaging system, was provided. If possible, sample experimental results were also provided to show the effectiveness of the BOS system in the respective ground test facility. For each of the entries presented in this paper, a discussion of the lessons learned from the implementation of the BOS technique was also provided in order to aid future BOS efforts in these, as well as other capability-related, ground test facilities. The purpose of this paper was to: (1) show that the BOS technique can be successfully implemented in NASA Langley ground test facilities and (2) provide guidance for future BOS entries in these facilities by identifying potential improvements to the respective BOS systems that may improve measurement sensitivities.

## Acknowledgements

Support for several of the tests described in this paper were conducted with the support of NASA's Aeronautics Test Program (ATP), Aeronautical Sciences Project (ASP), and the NASA Rotary Wing Project Office. The authors would like to thank Dr. Joel Everhart of NASA Langley Research Center for continual support and encouragement pertaining to the implementation of the Background-Oriented Schlieren technique in NASA ground test facilities. The authors would like to acknowledge Scott Murman (NASA Ames) for providing CFD density field data in support of the testing in the 13-Inch Low-Speed Wind Tunnel as well as Paul Danehy (NASA Langley) for facilitating that test entry.

## References

<sup>1</sup> Settles, G.S., *Schlieren and Shadowgraph Techniques*, 1<sup>st</sup> ed., Springer-Verlag, New York, NY, 2001.

- <sup>2</sup> NASA Aeronautics Test Program Brochure, available at <http://www.aeronautics.nasa.gov/atp/documents/B-1240.pdf>, accessed 6/2014.
- <sup>3</sup> Paryz, R.W., “Upgrades at the NASA Langley Research Center National Transonic Facility,” AIAA-2012-1450, 50<sup>th</sup> AIAA Aerospace Sciences Meeting, Nashville, TN, January, 2012.
- <sup>4</sup> Piatak, D.J., “Survey of Primary Flow Measurement Parameters at the NASA Langley Transonic Dynamics Tunnel,” NASA Technical Memorandum 2003-212413, June, 2003.
- <sup>5</sup> Florance, J.R., and Rivera Jr., J.A., “Sidewall Mach Number Distributions for the NASA Langley Transonic Dynamics Tunnel,” NASA Technical Memorandum 2001-211019, June, 2001.
- <sup>6</sup> Micol, J.R., “Langley Aerothermodynamic Facilities Complex: Enhancements and Testing Capabilities,” 38<sup>th</sup> AIAA Aerospace Sciences Meeting, AIAA 1998-147, 1998.
- <sup>7</sup> NASA Langley Aerothermodynamic Laboratory Fact Sheet, available at: [researchtech.larc.nasa.gov/resources/LAL\\_factsheet.pdf](http://researchtech.larc.nasa.gov/resources/LAL_factsheet.pdf), accessed 11/2014.
- <sup>8</sup> Rasband, W.S., ImageJ, U.S. National Institutes of Health, Bethesda, MD, USA, <http://rsb.info.nih.gov/ij/>, 1997-2009.
- <sup>9</sup> Murrill, R.J., “Operation and Maintenance Manual for the General Rotor Model System”, SER-50986, NAS1-12674, May 1977.
- <sup>10</sup> Li, K., *The image stabilizer plugin for ImageJ*, [http://www.cs.cmu.edu/~kangli/code/Image\\_Stabilizer.html](http://www.cs.cmu.edu/~kangli/code/Image_Stabilizer.html), February, 2008.
- <sup>11</sup> Mizukaki, T., Borg, S.E., Danehy, P.M., and Murman, S.M., “Visualization of Flow Separation Around an Atmospheric Entry Capsule at Low-Subsonic Mach Number using Background-Oriented Schlieren (BOS),” AIAA Paper 2014-2521, 30<sup>th</sup> AIAA Aerodynamic Measurement Technology and Ground Testing Conference, Atlanta, GA, June, 2014.
- <sup>12</sup> Danehy, P.M., Inman, J.A., Braukmann, G.J., Alderfer, D.W., Jones, S.B., and Patry, D.P., “Visualization of a Capsule Entry Vehicle Reaction-Control System Thruster”, *Journal of Spacecraft & Rockets*, Vol. 46(1), January – February, 2009.